

A Mechanism of Structure Driven Nonlinear Instability of Double Tearing Mode in Reversed Magnetic Shear Plasmas

M. Janvier 1), Y. Kishimoto 1), J. Li 1)

1) Graduate School of Energy Science, Kyoto University, Japan

E-mail contact of main author: janvier.miho@ay7.ecs.kyoto-u.ac.jp

Abstract. The nonlinear destabilization of the Double Tearing Mode (DTM) and its subsequent collapse have attracted much attention as a crucial problem which terminates high performance reversed magnetic shear plasmas. However, the underlying physical mechanisms, especially the trigger mechanisms, have not been fully understood. Here, we find possible responsible processes which are characterized by two distinct but coupled secondary instabilities. First, a *secondary instability* has been found to grow due to the magnetic topology deformation induced during the nonlinear evolution of the magnetic islands. This secondary instability can be associated to the growth of potential flows with fast time scale. Investigating cases near marginal stability, we also find that the secondary instability resembles a modulational instability, as its growth rate is directly related to the amplitude of the original two dimensional deformation of the magnetic islands. Also, we find that a strong zonal field ($m=0$ component of the flux) arises, leading to total reconnection of the magnetic field. Such strong zonal component can modify the original equilibrium profile and lead to new current instabilities as its alteration, *i.e.*, corrugations, can affect tearing mode stability. As the zonal field is generated by the coupling between destabilized flows and slowly evolving magnetic flux, the two possible mechanisms for the nonlinear destabilization of the double tearing mode are subsequently coupled, leading to strong kinetic flow growth and to full reconnection/collapse.

1. Introduction

High performance plasma with internal transport barriers (ITBs) have been observed in reversed magnetic shear configuration in tokamaks. However this configuration, associated to hollow current density profiles, sometimes leads to plasma discharge termination due to the sudden appearance of macro-scale MHD activities [1]. The double tearing mode (DTM), consisting in two unstable current sheets, has been considered as a plausible candidate to explain such phenomena, and has been observed to cause enhanced dynamics leading to disruptions or collapse [2]. First analyzed for two typical regimes, the $\gamma \sim \eta^{3/5}$ regime (tearing-like DTM for large separation of rational surfaces) [3] and $\gamma \sim \eta^{1/3}$ regime (kink-like DTM for small separation) [4], this particular MHD mode has since then been studied systematically for different rational surface separation lengths. Ishii et al. [5,6] and Wang et al. [7,8] found that for intermediate distances between tearing layers, the DTM evolution exhibits a nonlinear destabilization, *i.e.*, a nonlinear regime where kinetic and magnetic energies suddenly grow. Ishii et al. found this resulting explosive growth by performing simulations in cylindrical geometry for the mode $m/n=3/1$. However, similar behaviours have been found in slab geometry [7-10], proving the phenomenon universality. They explained the nonlinear DTM sudden growth as a structure-driven nonlinear instability generation due to the magnetic configuration deformation associated to magnetic islands growth. The importance of the Maxwell stress term in the MHD equations was emphasized in evaluating the current role compared to that of the flow. However, Wang et al. found that generation of intrinsic flows could be the origin of driven reconnection leading to faster time scale at the end of the nonlinear regime.

Here, by studying the DTM in slab geometry, we propose a new and deeper analysis of the problem by separately looking at the flow and flux roles. Conducting a secondary instability analysis, we have been able to identify the explosive growth as two different but

nonetheless correlated secondary instability processes with respect to the flow and flux on different time scales. First, two dimensional deformation of magnetic structures due to the growth of magnetic islands can destabilize modulational-type instabilities. Secondly, the strong zonal field that is generated via coupling of nonlinear flow and flux can play an important role in triggering new current instabilities through corrugations of the equilibrium.

2. Nonlinear simulation of DTM

2.1. Reduced MHD equations and configuration

We study the DTM nonlinear evolution based on the two-field reduced MHD equations for the potential ϕ and the flux ψ in slab geometry, assuming incompressibility of the flow and a strong guide field in the z -direction:

$$\partial_t \psi = -[\phi, \psi] + \eta \nabla^2 \psi, \quad (1)$$

$$\partial_t \nabla^2 \phi = -[\phi, \nabla^2 \phi] + [\psi, \nabla^2 \psi]. \quad (2)$$

The flux ψ and the potential ϕ are related to the magnetic field \vec{B} and the velocity field \vec{v} via $\vec{B} = \vec{e}_z \times \nabla \psi$ and $\vec{v} = \vec{e}_z \times \nabla \phi$, where \vec{e}_z is the unit vector in the parallel field direction. Time and length respectively have the unit of Alfvén time τ_A and of a specific length of the system a .

The configuration of the equilibrium magnetic field B_{oy} is chosen as $B_{oy}(x) = 1 - (1 - B_c) \cosh^{-1}(\xi x)$ [3]. The constants B_c and ξ are chosen so as to obtain $B'_{oy}(x_s) = J_{oy}(x_s) = \pi/2$ where $\pm x_s$ defines the positions of the rational surfaces. No initial flow is assumed ($\phi_0 = 0$). The equations are solved using a finite difference method in the x -direction. The box of length $[-5:5]$ is divided by 2048 mesh numbers with equal spacing ($\Delta x = 0.00489$). Conducting walls are chosen as boundary conditions in the x -direction. In the y -direction, perturbations are Fourier decomposed assuming periodical boundaries. The number of Fourier harmonics that is necessary to obtain full convergence depends on other parameters of the simulation such as the box size in the y -direction or the resistivity, but generally around 10 harmonics are enough to reproduce the dynamics of the DTM. In the present study, the distance between the rational surfaces is fixed as $2x_s = 1.60$, and the typical resistivity is $\eta = 10^{-4}$.

2.2. Typical dynamics of the nonlinear destabilization of the DTM

In this subsection, we present a typical case for the nonlinear destabilization of the DTM. The box size in the y -direction is chosen as $2\pi L_y = 2\pi \times 1.2$ with five Fourier harmonics for the spatial decomposition. The time evolution of the energies are given in Fig.1(a): the magnetic energy $E_M = |\psi|^2 / 2$ for $m=0$ (black solid line) and $m=1$ (red dashed line), and the kinetic energy $E_K = |\phi|^2 / 2$ for $m=1$ (green solid line). Extending the definition of the linear growth rate to the nonlinear regime ($\gamma_M = d_t(\ln(E_M))$), $\gamma_K = d_t(\ln(E_K))$, the instantaneous growth rates of the energies mentioned above are plotted in Fig.1(b).

The DTM starts with a linear evolution during which nonlinear couplings are weak. Note that $m=1$ is the only linearly unstable mode that drives the other Fourier harmonics growth (such as the zonal field $m=0$) in the nonlinear regime. The linear stage ends around $t = 500\tau_A$ and is followed by a slow down similar to the Rutherford stage [11] in the classical

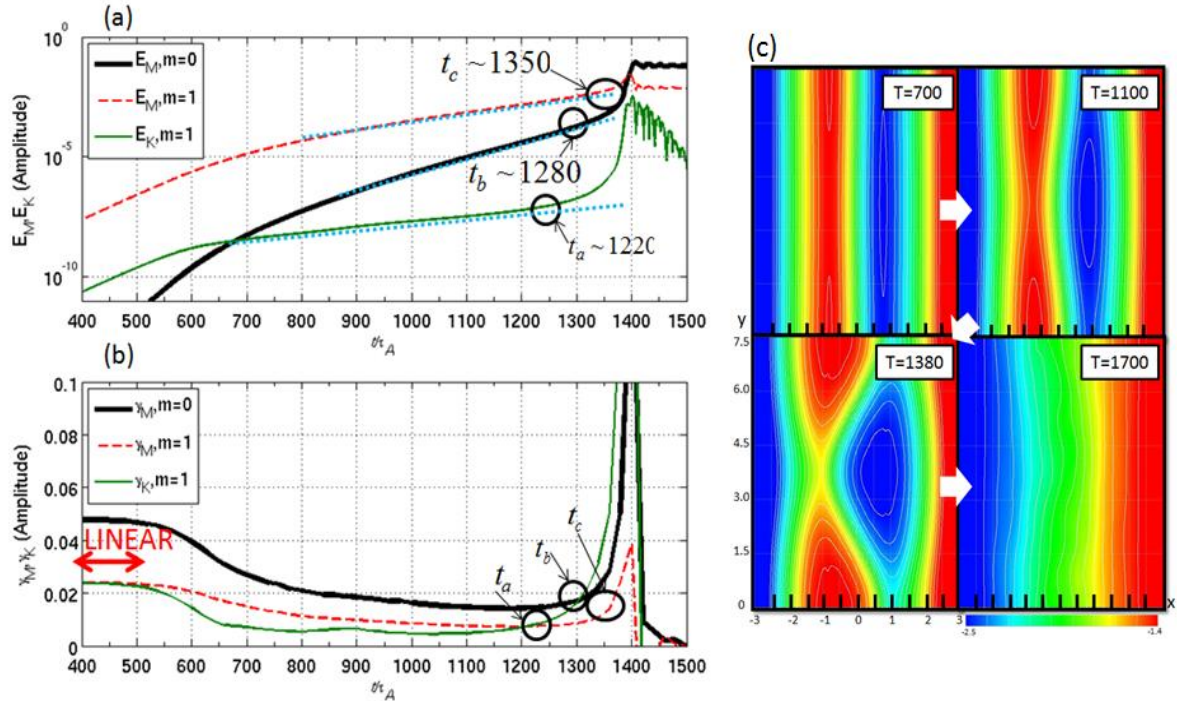


Fig.1.a) Evolution of magnetic and kinetic energies b) Equivalent instantaneous growth rates c) Corresponding evolution of magnetic field topology

tearing instability. In this latter phase, the flux continues to increase in time while the flow evolves much slowly, suggesting a decoupling between magnetic flux and potential flow. However, contrary to a typical single tearing mode, the energies do not saturate but instead grow again up to roughly $t \sim 1300\tau_A$ when they enter an abrupt growth regime. The corresponding evolution of the magnetic field topology (contour plot of ψ function) at selected times is given in Fig.1(c). In the slow-down regime, small and elongated magnetic islands start to appear and continue to grow. During the fast growth regime, the islands are well developed and lose their symmetry in regards to their relative current layer: their growth mutually deforms each other. The abrupt growth is terminated when the zonal field harmonic ($m=0$) reaches a higher energy amplitude than the dominant mode $m=1$. This corresponds to total reconnection of magnetic field line as shown in Fig.1.3 (bottom left image) where the two tearing layers have completely disappeared.

Now, looking in more details at the flow and the flux energy evolutions, they seem to follow different dynamics: first, around $t_a \sim 1220\tau_A$, $E_K(m=1) = |\phi_{m=1}|^2$ abruptly increases and is followed, around $t_c \sim 1350\tau_A$, by $E_M(m=1) = |\psi_{m=1}|^2$ with a smaller growth rate. More interestingly, $E_M(m=0) = |\psi_{m=0}|^2$ also starts to increase with a delay from time t_a , i.e. around $t_b \sim 1280\tau_A$. In Fig.1.(b), where the instantaneous growth rates are plotted, the causality relation $t_a < t_b < t_c$ can also be seen. The DTM nonlinear destabilization leading to subsequent fast growth of energies may be understood as the triggering of new instabilities. To investigate such idea, we conduct a secondary instability analysis.

3. Modulational-type secondary instability

3.1. Numerical method for a secondary instability analysis

The secondary instability analysis consists in investigating a subsequent instability growth from a primary instability saturated quasi-steady state. This study is for example

relevant to the investigation of zonal flow generation mechanisms in a saturated turbulent background [12]. Here, the primary instability is the DTM and the quasi-steady states correspond to the magnetic configurations such as represented in Fig.1(c): structures at different times in the slow-down regime correspond to quasi-steady equilibria with more or less developed magnetic islands. The evolution of the instantaneous growth rates of the magnetic and kinetic energies justify this choice. As seen in Fig.1(b), they decrease from their linear value $\gamma_{lin} \sim 0.025$ to a lowest one during the nonlinear slow-down, before increasing again. The growth rates remain around their smallest value from $t_s \sim 900\tau_A$ to $t_f \sim 1250\tau_A$, suggesting a quasi-steady state and making possible a secondary instability analysis. To study the stability of an equilibrium with two-dimensional islands, we employ the same magnetic island structures as those obtained during the DTM nonlinear evolution. We define several equilibria corresponding to magnetic islands with different sizes, such as in Fig.1(c).

Numerically, the secondary analysis implies linearly solving the RMHD equations with a two-dimensional new equilibrium (x and y directions with magnetic islands) [9,10] given by:

$$\partial_t \tilde{\psi} = -[\tilde{\phi}, \psi_E(x, y)] - [\phi_E(x, y), \tilde{\psi}] + \eta \nabla^2 \tilde{\psi} \quad (3)$$

$$\partial_t \nabla^2 \tilde{\phi} = -[\tilde{\phi}, \nabla^2 \phi_E(x, y)] - [\phi_E(x, y), \nabla^2 \tilde{\phi}] + [\tilde{\psi}, \nabla^2 \psi_E(x, y)] + [\psi_E(x, y), \nabla^2 \tilde{\psi}]. \quad (4)$$

The equations above are similar to the usual RMHD equations, although now new infinitesimal perturbations $\tilde{\psi}$ and $\tilde{\phi}$ are evolving under the new equilibrium ψ_E and ϕ_E . Note that due to this specific equilibrium, perturbations are linearly coupled with each other via the Poisson brackets. Therefore, all newly generated harmonics are evolving with the same linear growth rate, leading to a global mode. To make the study self-consistent, ψ_E, ϕ_E and their radial derivatives (B_E, J_E, \dots) are taken from the DTM nonlinear evolution of part 2 (Fig. 1) at selected times. As we study several magnitudes of magnetic islands deformation, the magnetic island width refer to corresponding different equilibria (calculated during the nonlinear evolution of the DTM).

3.2. Typical case for the secondary instability analysis

The time evolution of the magnetic island width, corresponding to the case studied in Part.2 ($2\pi L_y = 2\pi \times 1.2$), is plotted in Fig.2(a). Note that from $t \sim 500\tau_A$ to $t \sim 800\tau_A$, a linear time dependency confirms the Rutherford-type evolution, such as for the single tearing mode. Also, even though the DTM corresponds to the growth of two magnetic islands on their respective rational layer, we will only refer to *one* magnetic island as their evolution is completely equivalent. When conducting the secondary instability analysis, we provide new equilibria with already developed magnetic taken from the DTM nonlinear evolution. The equations are solved as an initial value problem with infinitesimal perturbations $\tilde{\psi}$ and $\tilde{\phi}$. Every equilibrium corresponding to the nonlinear magnetic configuration is found to be unstable. However, the linear growth rate of the perturbations depends on the two-dimensional structural shape. This growth rate has been plotted in function of the equilibrium island width in Fig.2(b) (y -axis in logarithm scale). Note that for an equilibrium with no magnetic islands ($w = 0$), the growth rate is the same as the linear DTM as the current sheets remain unmodified. Then, two phases can be seen: first, the growth rate decreases when the magnetic islands grow, up to $w \sim 0.6$. This suggests that small and thin magnetic islands such as in the slow-down DTM nonlinear regime have a stabilizing effect. However, from $w \sim 0.6$, the linear growth rate of the perturbations starts increasing, suggesting that large magnetic islands can play a destabilizing role. The width $w \sim 0.6$ corresponds to the time

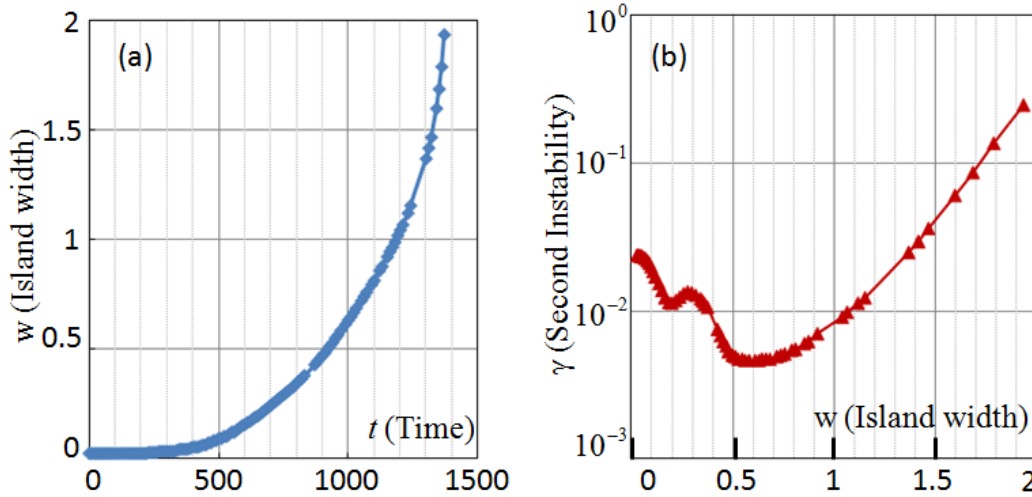


Fig.2.a) Time evolution of magnetic island width b) Second instability growth rate in function of the equilibrium island width

$t \sim 1000\tau_A$ in the nonlinear calculation. Therefore, during the development of the DTM, a secondary instability starts growing around $t \sim 1000\tau_A$ but is still weak so that its evolution is masked due to other nonlinear processes that may work as dissipation. Comparison between the secondary instability growth rate and the instantaneous growth of potential flows shows similarities, suggesting that when the new instability becomes strong, its evolution can be seen in that of the flow (In Fig.1 around $t \sim t_a$). Also, with rough estimations, the size of thin magnetic islands can be approximated by $w \sim \sqrt{\psi}$. Although such relation may not stand for larger magnetic islands, we suggest that the growth rate of the second instability can depend on the flux amplitude, similarly to a *modulation instability* which generates a zonal flow component from a turbulent background. To further investigate such relation, we conduct new studies for cases of nonlinear DTM that are near marginal stability.

3.3 Case near marginal stability

When conducting a systematic study for the DTM, we found that linearly unstable modes with small linear growth rates yield subsequent dynamics with no nonlinear destabilization. The selection of such modes corresponds to the reduction of the box size in the y-direction: as the

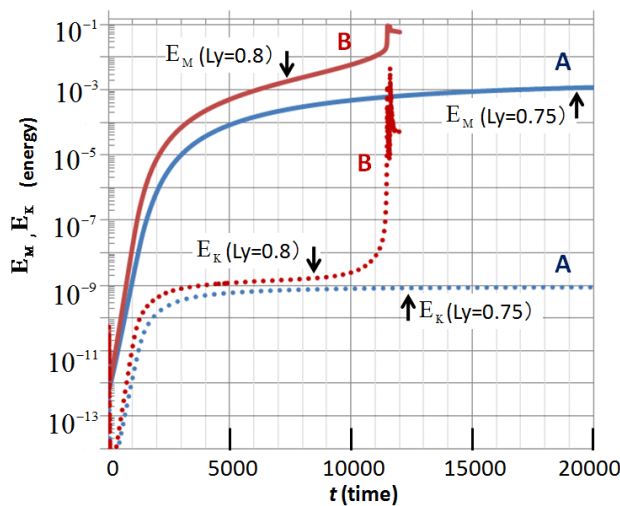


Fig.3: DTM nonlinear evolution for $L_y=0.75$ and $L_y=0.8$

DTM linear growth rate depends on the wavenumber k (itself related to the poloidal length of the box size via $k = L_x m / 2\pi L_y$), decreasing the length can excite small wavelengths, which are more stable to current destabilization. In the case of section 3.2 ($2\pi L_y = 2\pi \times 1.2$), the dynamics is therefore fast compared to smaller box size configurations as seen in Fig.3. In this figure, we have plotted the evolution of the total magnetic (plain curve) and kinetic (dotted curve) energy for $2\pi L_y = 2\pi \times 0.75$ (case A, in blue) and $2\pi L_y = 2\pi \times 0.8$ (case B, in red) (with ten poloidal Fourier harmonics).

For $L_y = 0.75$, the kinetic energy as well as the magnetic energy reach saturation after the slow-down during the nonlinear regime. With $L_y = 0.8$ however, the dynamics returns to nonlinear stability as observed in $2\pi L_y = 2\pi \times 1.20$ case. This suggests that there is a critical box size within $0.7 < L_{yc} \leq 0.8$ from which the nonlinear DTM destabilization is systematically triggered. Note that compared with case $L_y = 1.2$, the dynamics for $L_y = 0.8$ is very long as the nonlinear slow down continues up to $t \sim 10000\tau_A$.

The same investigation of the secondary instability as in the part 3.2 is conducted for $L_y = 0.8$ [10] and the results are plotted in Fig.4 for different equilibria (corresponding to different magnetic island widths, equivalent ψ_E, ϕ_E of case B simulation). Here also, the growth rate is shown on a logarithmic scale. Up to $w \sim 0.8$, the linear growth rate decreases as the small magnetic islands slightly modify the current sheets. Again, this can be understood as there is less free energy due to the quasi-linear current flattening in the Rutherford regime. However, this growth rate rapidly and discontinuously increases from $w \sim 0.8$. This feature clearly displays the appearance of a *secondary instability*, its energy source being different from that of the linear instability, *i.e.* a current gradient.

Interestingly, the growth rate of this instability is found to evolve exponentially with the magnetic island width (linearly in logarithm scale as in Fig.4). Then, roughly estimating this width as $w \sim \sqrt{\psi}$, the linear growth rate of the secondary instability can now be linked to the magnetic flux amplitude: $\gamma_s \sim e^{\sqrt{\psi}}$. This exponential dependence has not been detected as clearly in previous simulations far above marginal stability [9], but is determined for the first

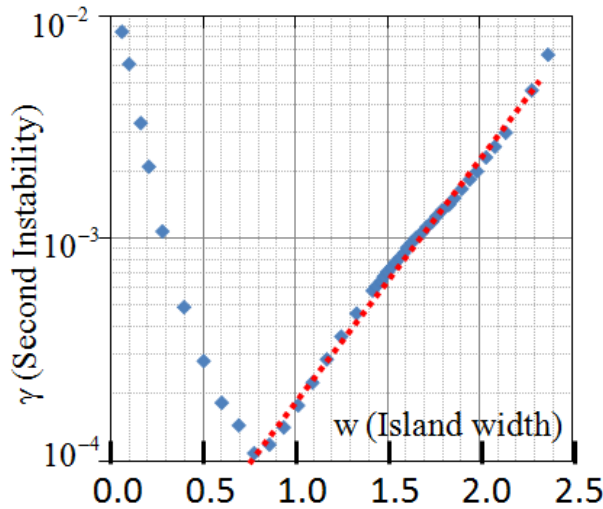


Fig.4: Second instability growth rate in function of the equilibrium island size ($L_y=0.8$)

time in the present simulation near marginality. The time evolution of the magnetic island width (*not presented here*) shows that the critical width $w \sim 0.8$ (from which the secondary instability grows) corresponds to $t \sim 5000\tau_A$ in the DTM nonlinear simulation (Fig.3). Comparing the flow instantaneous growth rate and the secondary instability one, we found that they become comparable around $t \sim 10000\tau_A$. Again, the secondary instability can start to grow around $t \sim 5000\tau_A$, but its evolution becomes detectable in the nonlinear simulation only around $t \sim 10000\tau_A$, in the evolution of the kinetic flows.

4. Zonal field driven secondary instability

The DTM nonlinear growth is abruptly ended when the $m=0$ magnetic energy component reaches the same level as the dominant $m=1$ one, leading to total reconnection. The $m=0$ harmonic generation (referred to as a zonal field) is possible via nonlinear coupling of other harmonics $m > 0$ ($\partial_t \psi_0 = -[\phi_{\pm m}, \psi_{\mp m}] + \eta \nabla^2 \psi_0$), and affects the equilibrium profiles. Whereas the resulting total radial profile of the poloidal magnetic field appears smooth, it has in fact small corrugations. Thus, radial divergences or gradients of this profile have large local variations. The subsequent highly corrugated current profiles can affect tearing mode stability [13]. Following those considerations, it is of primary importance to understand what the direct effects on the equilibrium profile are, and if resulting modifications can affect current instability developments in the DTM nonlinear dynamics. Furthermore,

when conducting the secondary instability analysis, structure deformations in the y -direction due to harmonics $m>0$ as well as radial characteristics are included. Those latter come either from harmonics $m>0$ or from the $m=0$ component itself. Therefore, we propose here to investigate this specific term. To reproduce local variations of magnetic field gradients, necessary convergence has been obtained by increasing Fourier harmonics in the y -direction up to $m_{tot} = 50$. In the present case, $L_y = 1.2$ and $\eta = 5 \times 10^{-4}$ are chosen for an easier computation. The profile time evolutions for the modified current $J_{eq} + J_{m=0}$ and its x -gradient $J'_{eq} + J'_{m=0}$ are plotted respectively in Fig.5(a) and 5(b). Although the energy time evolution is not shown, the original current profile J_{eq} (black solid line, Fig.5(a)) do not present any change at $t \sim 200\tau_A$ (orange dashed line) (linear stage), is being flattened by $m=0$ at $t \sim 300\tau_A$ (red solid line) (slow down regime), and from $t \sim 400\tau_A$, a peaked profile appears, correlated to strongly localized corrugations of J' (blue and green curves in Fig.5(a) and 5(b)) (nonlinear destabilization phase). Those corrugations can influence the evolution of tearing modes: when looking at the quasi-linear equations for $m>1$,

$$\partial_t \psi_{m>0} = \partial_y \phi_{m>0} \partial_x (\psi_{eq} + \psi_{m=0}) + \eta \nabla^2 \psi_{m>0} \quad (5)$$

$$\partial_t \nabla^2 \phi_{m>0} = -\partial_y \psi_{m>0} (J'_{m=0} + J'_{eq}) + \partial_x (\psi_{eq} + \psi_{m=0}) \partial_y J_{m>0}, \quad (6)$$

the term $J'_{eq} + J'_{m=0}$ plays an important role.

To confirm this idea, we proceed to the numerical investigation of infinitesimal perturbations linearly evolving under equilibrium profiles defined as $X_{new} = X_{eq} + X_{m=0}$ (where $X = \psi, B, J$). They actually correspond to the profiles in Fig.5. We reported in Fig.6 the linear growth rate (blue circles) of the resulting linearly unstable mode $m=1$ for each profile taken from the original DTM simulations at $t = 0, t = 200\tau_A, t = 300\tau_A, t = 400\tau_A$ and $t = 450\tau_A$. We also added the growth rates corresponding to the original simulation with the same parameters except the total Fourier harmonics ($m_{tot} = 20$). Note that convergency is assured as same results are found. At $t = 200\tau_A$, the current profile being unmodified, the resulting growth rate is the same as in the linear stage of the DTM. At $t = 300\tau_A$, the linear growth rate decreases: as the $m=0$ component flattens the current profile (Fig.5(a)), there is less free energy available for a current destabilization. The minimum for the linear growth rate would be found for a modified equilibrium at $t = 350\tau_A$ (run for $m_{tot} = 20$). However, for

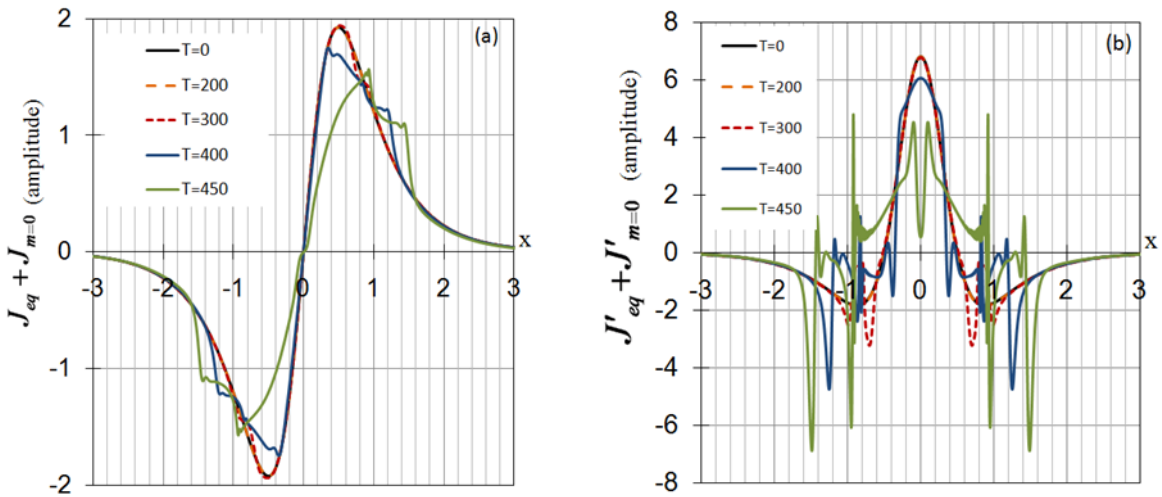


Fig.5.a) Profile evolution of the equilibrium current modified by zonal components

b) Profile evolution of J' (derivation of the current in the x direction)

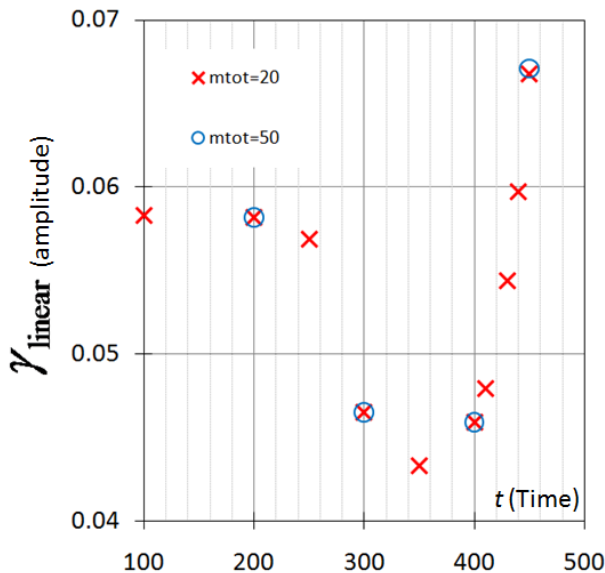


Fig 6. Linear growth rate for different equilibria modified by zonal field components

$t = 400\tau_A$ and $t = 450\tau_A$, the linear growth rate of the new perturbation increases and from $t = 420\tau_A$, becomes even higher than the linear DTM growth rate. Then, the corrugations of the zonal field profile and especially of its derivatives ($J_{m=0}$ and $J'_{m=0}$) affect the original equilibrium profile. This latter can therefore drive new instabilities. We refer to this instability as a *zonal field driven tearing instability*. This may contribute to enhanced nonlinear dynamics leading to the fast growths observed in the DTM nonlinear destabilization.

Conclusion

To investigate the possible mechanisms leading to the DTM nonlinear destabilization, a secondary instability analysis with two-dimensionally modified quasi-steady equilibrium has been conducted near and far from marginal nonlinear stability of the DTM dynamics. The results show that two-dimensional structure deformations due to growing magnetic islands can explain the generation of a modulational-like instability which evolution can be linked to the growth of kinetic flows. Resulting nonlinear coupling with magnetic flux may lead to current corrugations of the equilibrium. A further study showed that such modifications can be the origin of current driven instabilities. These and modulational-type secondary instabilities are taking place subsequently, and a causality relation might exist between flow and flux evolution, such as discussed in Part 2, leading to the full reconnection of magnetic field lines.

References

- [1] MAGET P. et al., *Nuclear Fusion*, **46** 797 (2006)
- [2] CHANG Z., et al., *Physical Review Letters*, **77** 3553 (1996)
- [3] PRITCHETT P.L., et al., *Phys. Fluids*, **23** 1368 (1980)
- [4] BIERWAGE A., et al., *Phys. Plasmas*, **14** 022107 (2007)
- [5] ISHII Y., et al., *Physical Review Letters*, **89** 205002 (2002)
- [6] ISHII Y., et al., *Nuclear Fusion*, **43** 539 (2003)
- [7] WANG Z.X., et al., *Physical Review Letters*, **99** 185004 (2007)
- [8] WANG Z.X., et al., *Phys. Plasmas*, **15** 082109 (2008)
- [9] JANVIER M., et al., (Proc. 19th Int. Toki Conf. 2010) *Plasma and Fusion Research*, **5** S2056 (2010)
- [10] JANVIER M., et al., *Plasma and Fusion Research (to be published)*
- [11] RUTHERFORD P.H., et al., *Phys. Fluids*, **16** 1903 (1973)
- [12] ROGERS B.N., *Physical Review Letters*, **85** 5336 (2000)
- [13] MILITELLO F., et al., *Phys. Plasmas*, **16** 032101 (2009)